北京大学

Undergraduate Dissertation

Title: Effect of Electron Beam Irradiation on the Magnetic Properties of Two-Dimensional LMO Thin Films

Name : Hao Li

Student ID : 1400011443

Department : School of Physics

Major : Physics

Supervisor : Jinbo Yang

May, 2018

Effect of Electron Beam Irradiation on the Magnetic Properties of Two-Dimensional LMO Thin Films

Abstract: Perovskite oxide, represented by perovskite manganese oxide, is a typical kind of material of strongly correlated system. Its abundant properties of superconductivity, colossal magnetoresistance, etc., provide a broad research platform for basic physics research. It is also demonstrated to be of great potential in many fields, such as storage, detection and spintronics. In this article, high quality $LaMnO_3$ (LMO) thin films grown on $SrTiO_3$ (STO) (001) substrates were selected as the research object, dealt with electron beam irradiation, and the changes in the magnetic properties of the samples before and after irradiation were studied. We try to explain the experimental phenomena by the effect of superexchange interactions, double exchange interactions, and exchange bias. It was found that after the electron beam irradiation, the sample was transformed from a single ferromagnetic phase to two ferromagnetic phase and an antiferromagnetic phase at low temperature (10K). The coercivity increased obviously, and the exchange bias effect appeared, while the ferromagnetism was weaker than the original sample. The samples are still ferromagnetic at high temperature and the minimum coercivity is near the point of transformation. In the experiment, the ratio of trivalent and tetravalent manganese ions of the sample before and after treatment were measured by XPS analysis, and we preliminarily suppose through STEM image that the diffusion process of the substrate may appear. The experimental phenomena can be explained preliminarily through this data and two indirect exchange interactions.

Key words: LMO, magnetic properties, electron beam irradiation, exchange interaction, exchange bias

Content

§1 Introduction

Perovskite oxides represented by perovskite manganate are a typical kind of strongly correlated materials. Due to their superconductivity [1], colossal magnetoresistance (CMR) [2], anomalous Hall effect [3], multiferroic [4], they provide a broad research platform for basic physics research, and also show great application prospects in storage, detection, spintronics and many other fields [5]. Since the 1950s, increasing attention has been paid to the crystal structure, magnetic and transport properties of perovskite oxides, and a lot of theoretical as well as experimental exploration has been carried out. Meanwhile, anomalous phenomena, such as insulator-metal transition [6], ordering [7] and phase separation [8], induced by the strong interaction, between charge, spin, orbit, and lattice, in perovskite manganate, has become a very active frontier in condensed matter physics in recent years.

The magnetism of perovskite manganate is closely related to the various interaction between electrons. In this paper, we will take $LaMnO_3$ as an example to study the relationship between its magnetism and electron interactions, using the electron beam irradiation to modify its magnetic properties.

1.1 Perovskite oxide

1.1.1 Structure

Ideal perovskite oxide ABO_3 has a simple cubic lattice, the space group of which is a cubic symmetric P_{m3m}, where A and O lie in cubic close packing, while B and its six nearest neighbor O atoms form a BO_6 octahedron. There are two ways of drawing methods, when taking A or B as center.

Real ABO_3 tends to distort into rhombohedral, orthorhombic or even monoclinic structure. It is generally believed that there are two reasons for the distortion of ABO_3 lattice: one is the mismatch between adjacent layers caused by the large difference of ion radius at A and B sites, which is a kind of stress effect; the other is the Jahn-teller

instability of B (d^4) ions, causing the distortion of oxygen octahedron (Jahn-teller distortion [9]), which is an electro-acoustic interaction. The ideal rare earth manganate $RMnO_3$ has a natural perovskite structure, generally being an antiferromagnetic insulator. Oxygen content, doping at A or B site, temperature and pressure can all deviate the lattice from the ideal perovskite structure. In some cases, sudden changes may occur, resulting in variation in the magnetic properties strongly associated with structure.

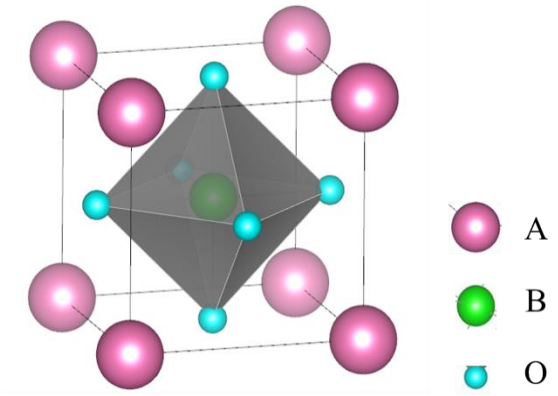

Fig.1.1 Crystal structure of ideal perovskite oxide ABO_3

To describe the extent of the extortion of the crystal structure of perovskite ABO_3, tolerance factor is introduced [10]:

$$f = \frac{r_A + r_O}{\sqrt{2}(r_B + r_O)} \tag{1}$$

where r_A, r_B, r_O are respectively the average radius of ions on A, B, and O sites. This factor reflects how well the matching is between the adjacent AO and BO_2 layers, and describes the deviation between the actual lattice and the ideal cubic lattice. Only when $0.9 < f \leq 1$ can stable perovskite structure be maintained [11]. When deviated from 1, the oxygen octahedron will rotate or tilt, resulting in structural distortion.

By doping with ions of different radius at A or B site, we can get a series of perovskite oxide with distinct crystal and electronic structure. By doping with ions of different radius at A or B site, we can get a series of perovskite oxide with distinct crystal and electronic structure. For doped rare earth manganate, usually a slight

deviation from ideal condition could sufficiently lead to transition of crystal structure to rhombohedral or orthorhombic system, with lower symmetry. As the tolerance factor or the ion radius of A site goes down, the crystal structure will first transform into rhombohedral, then orthorhombic. In these two structures, the bond length of Mn-O-Mn changes, so the bond angle departure from 180° for ideal structure, affecting the interactions between nearby Mn ions, and eventually affect the magnetism. As bond angle decreases, Curie temperature also reduces with it [12].

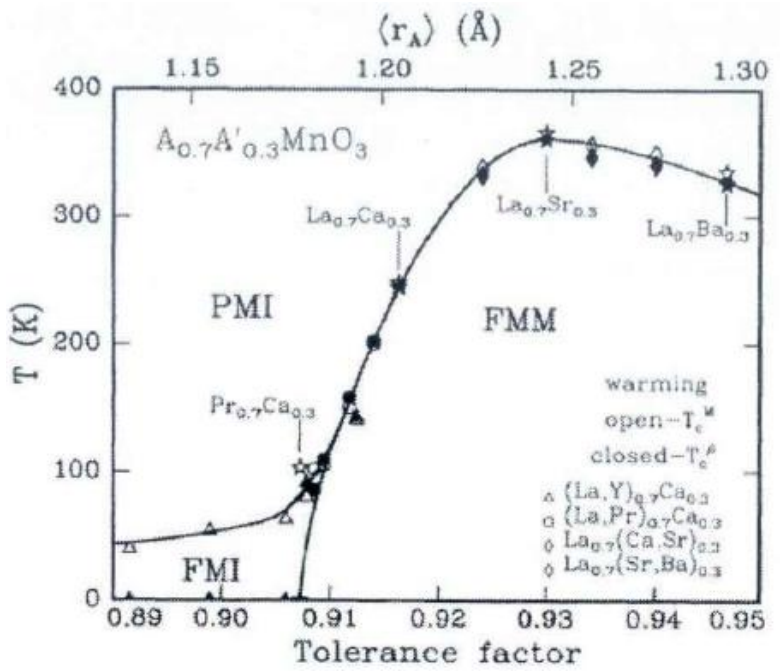

Fig.1.2 The relationship between Curie temperature and the tolerance factor in $R_{0.7}A_{0.3}MnO_3$ systems

1.1.2 Jahn-Teller distortion

In the ideal perovskite manganate, Mn is located at the center of MnO_6 octahedron, and the cubic symmetry of crystal field leads to the splitting of the 3d energy level, with fivefold degeneracy for free Mn ions, into two levels of e_g and t_{2g}. In the former case, it is double degenerate and high in energy; while the latter is triple degenerate and also of high energy. Therefore, the whole system still has high energy.

In 1937, Jahn and Teller put forward [9], because Mn^{3+} ions have four electrons, one is distributed in the higher e_g level, and the other three are distributed in the lower

t_{2g} level, the overall energy is still high. In order to reduce the internal energy, lattice distortion is required, resulting in the splitting of degenerate e_g and t_{2g} energy levels respectively, while the t_{2g} level splits into a single state with lower energy and a double degenerate state with higher energy. For Mn^{2+} and Mn^{4+}, however, energy level is either half filled, or e_g is empty, so there is no such distortion, and t_{2g} level is still degenerate [13] for them.

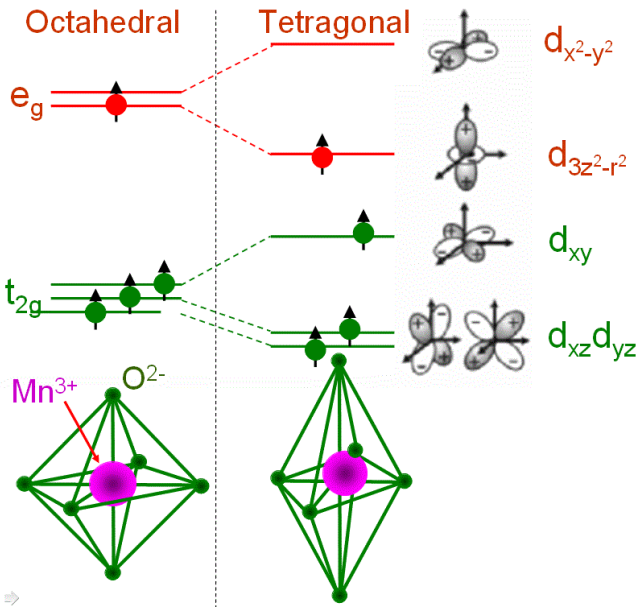

Fig.1.3 The electronic structure of Mn^{3+} ions, and the energy level split due to Jahn-Teller effect

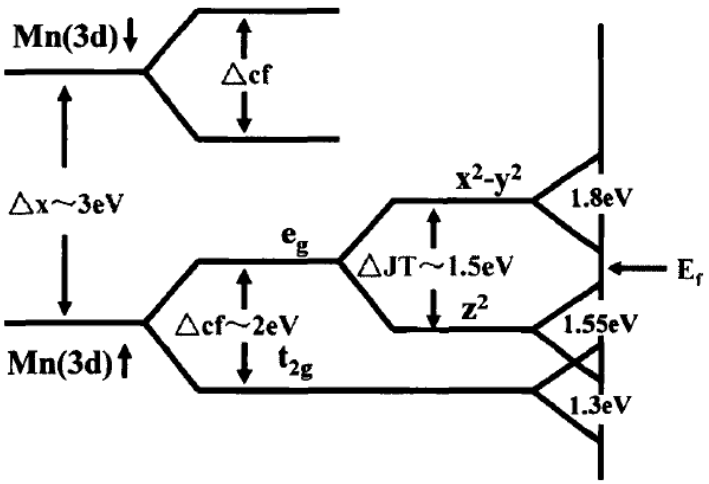

Fig.1.4 The energy level split by Jahn-Teller effect (take LMO as an example)

For example, for $La_{1-x}Ca_xMnO_3$ and $La_{1-x}Sr_xMnO_3$, where $x = 0.2\sim0.5$, the amount of Mn^{4+} is high, so some of the e_g levels are empty, thus reduces Jahn-teller effect, and inducts the crystal structure to high symmetry. For systems with Mn^{3+} and Mn^{4+} together, ferromagnetism and metallicity will emerge.

1.2 Interactions between electrons

1.2.1 Direct exchange interaction

Heisenberg proposed the exchange interaction model of ferromagnetism, based on the discussion of the exchange interaction term of hydrogen atom's binding energy in quantum mechanics [14], and believed that the spontaneous magnetization of ferromagnetism originated from the electrostatic exchange interaction between electrons.

The interaction energy between spins of atoms in the system is [15]:

$$\hat{H}_{\text{ex}} = -2\sum_{i<j} A_{ij}\hat{S}_i \cdot \hat{S}_j \tag{2}$$

where

$$A_{ij} = \frac{1}{(2S)^2}\sum_{p,q} A_{ip,jq} \tag{3}$$

is the exchange integral. $\hat{S}_i = \sum_p \hat{\sigma}_{ip}$ and $\hat{S}_j = \sum_q \hat{\sigma}_{jq}$ are the total spins for atoms with unfilled energy levels, i.e. with atomic magnetic moment, involved in exchange interaction. S is the quantum number for spin angular momentum.

Heisenberg further simplified this N atom system, only considering exchange interaction between different atoms, and only one electron in the outermost shell of each atom contributed to ferromagnetism [16]. For the above case, $S = \frac{1}{2}$, and only the nearest neighbor interaction is considered meanwhile $A_{ij} \to A_{i,i\pm1} = A$. For far away atoms, $A_{ij} = 0$, so formula (2) is simplified as

$$\hat{H}_{\text{ex}} = -2A\sum_{\text{n.n.}} \hat{\sigma}_i \cdot \hat{\sigma}_j \tag{4}$$

When the system is the most stable at ground state, requiring $H_{\text{ex}} < 0$. When

$A<0$, $(S_i \cdot S_j)<0$, the ground state is that the spins for nearest atoms are antiparallel, i.e. antiferromagnetic state; while when $A>0$, $(S_i \cdot S_j)>0$, the ground state is when spins for nearest neighbors are parallel, i.e. ferromagnetic state. Therefore, if spontaneous magnetization (i.e. all the spins are parallel) occurs, there must be $A>0$, which depends on the distance R_{ij} between two atoms, the distance r_i and r_j between the electron and the two atoms, and the characteristics of wave function [17].

Bate and Slater estimated the relationship between the exchange integral A and the ratio of the atomic spacing R and the radius r of 3d or 4f orbit based on the above theory [18]. The relation between exchange integral A and a/r_{3d}, given by Bethe and Slater, is shown in Fig. 1.5. When the ratio a/r is large, then A is positive, but $A \ll kT$, so it is paramagnetic, which is common for rare earth metals; with a/r decreasing, ferromagnetism occurs; go on reducing the exchange integral so that $A<0$, then the spins for nearest neighbor electrons will be antiparallel, so that antiferromagnetism emerges [17].

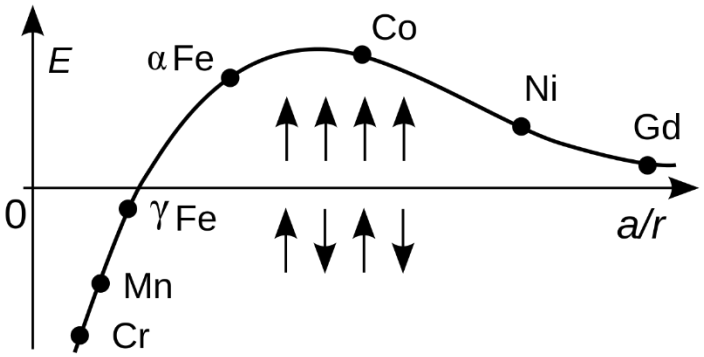

Fig.1.5 The relationship between exchange integral A (here is E) and a/r, given by Bethe and Slater

The Curie temperature for ferromagnets are proportional to exchange integral [19]

$$T_c = \frac{2ZA}{3k} \tag{4}$$

In fact, Curie temperature is the macroscopic representation of the strength of exchange

interaction in a ferromagnet. The stronger the exchange interaction, the greater the tendency for the spins to be parallel to each other, and thus the higher the energy is required to destroy the regular arrangement in the magnet, and macroscopically, the higher the Curie temperature is. Although for Fe, the calculated Curie temperature $T_C \approx 100\text{K}$, deviates quite a bit from the reality [20], indicating that Heisenberg theory can only give qualitative results, it is still practical in understanding the nature of molecular field and solving the problem of magnetism [17].

Fig. 1.6 shows the relation between exchange integral A and $R-2r$ for some metals and alloys, proposed by Neel. When $R-2r$ is large, the Curie temperature is low; for smaller $R-2r$, the system is antiferromagnetic. The results of the two graphs are basically the same in nature, being similar in shape, while only slightly different in abscissa. Although the theory is greatly approximate, but from the point of view of distinguishing ferromagnet and antiferromagnet, it is consistent with the reality.

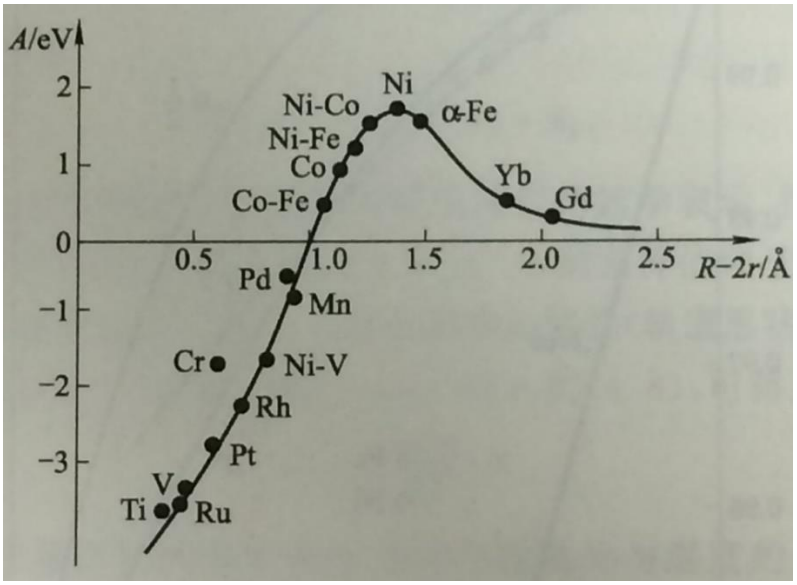

Fig.1.6 The relation between exchange integral A and $R-2r$ for some metals and alloys, proposed by Neel

We can use the curve above to explain some experimental phenomena [17], for example, we can change the structure of matter or change the atomic spacing to make $A>0$, to produce new ferromagnetic materials. And for example, Mn usually behaves

as an antiferromagnet, Bi is a diamagnetic metal, but the equal mixture alloy MnBi is ferromagnetic, with $T_c = 358℃$. This is because the atomic spacing of Mn in the alloy is larger than that in the pure metal, a/r_{3d} increases, so the exchange integral becomes positive. However, in fact, the exchange interaction between 3d electrons in 3d metals is generated by itinerant electrons, whose properties depend on the band structure. Therefore, there are many defects in this theory, and some characteristics of the curve deviate from the experiment.

1.2.2 Superexchange interaction

Most of the antiferromagnets or ferrimagnets are insulating compounds, the cations of which are generally transitional metals, and the nearest neighbors are anions. Therefore, the metal ion spacing is large, with almost no overlap of electron shells, so the direct exchange action is very weak, which is not suitable for such compounds [21].

In 1934, Kramers introduced a superexchange (indirect exchange) model to explain the origin of spontaneous magnetization of antiferromagnetism [22]. In 1950, Anderson developed histheory [23], calculated the superexchange interaction, and applied it to ferrimagnetism. A set of semi-empirical rules were also developed by John B. Goodenough and Junjiro Kanamori in the 1950s, now referred to as the Goodenough–Kanamori rules, have proven highly successful in rationalizing the magnetic properties of a wide range of materials on a qualitative level.

Taking the MnO as an example, where O^{2-} ions are in the middle of Mn^{2+} ions. There are two kinds of Mn^{2+}-O^{2-}-Mn^{2+} coupling, with bond angle of $180°, 90°$ respectively. The structure of the extra-nuclear electrons for O^{2-} ion is $1s^2 2s^2 2p^6$. The p-orbital overlaps with the neighboring Mn^{2+} ions, labelled M_1 and M_2, so a p-electron transfer to the 3d orbital of M_1. Since each Mn^{2+} ion has five half-filled levels already, according to Hund's rule and Pauli Exclusion Principle, the p-electron spin of the intermediary non-magnetic O^{2-} can only be antiparallel to the five spins of Mn^{2+}. At the same time, the remaining spin in the p-orbit must be antiparallel to the transferred spin,

so then the exchange interaction between M_2 will cause the p-electron spin to be antiparallel to the d-electron spin of M_2, resulting in the antiparallel of M_1 and M_2 spins or say strong antiferromagnetism, while in another case, the coupling between an ion with a filled orbital and one with a half-filled orbital will generally be ferromagnetic. This kind of exchange interaction is mediated by oxygen ions, which is called superexchange. When multiple types of interactions are present simultaneously, the antiferromagnetic one is generally dominant since it is independent of the intra-atomic exchange term. For simple cases, the Goodenough–Kanamori rules readily allow the prediction of the net magnetic exchange expected for the coupling between ions.

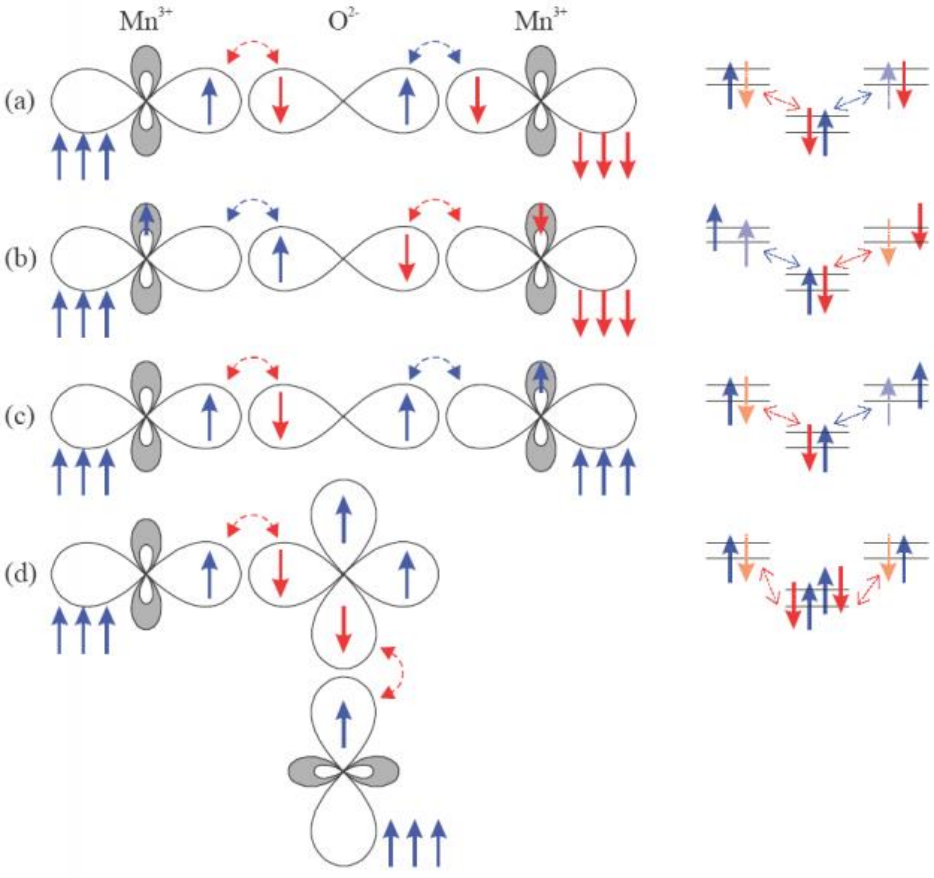

Fig.1.7 The Goodenough-Kanamori-Anderson rules of superexchange interaction, in MnO

For the vast majority of antiferromagnetic and ferromagnetic materials [24], according to Hund's rule, when the number of 3d electron of M_1 is less than 5, the p-

electron spin in the excited state will be parallel to the 3d spin of M_1. On the contrary, if the number of 3d electron of M_1 is greater than or equal to 5, they will be antiparallel. Since 2p electron pair has antiparallel spins, the remaining p-electrons will have a negative exchange interaction with d electrons in M_2. When the angle $M_1\text{-}O\text{-}M_2 = 180°$, the superexchange interaction is the strongest, and when the angle is smaller, the superexchange is weaker. Ions super exchange with O^{2-} ions are both Mn^{2+}, with negative exchange integrals. The spins of coupling electrons is therefore antiparallel, which leads to antiferromagnetism.

What is relevant to the content of this paper is that the model can also be used to explain that the undoped LMO is a type-A antiferromagnet.

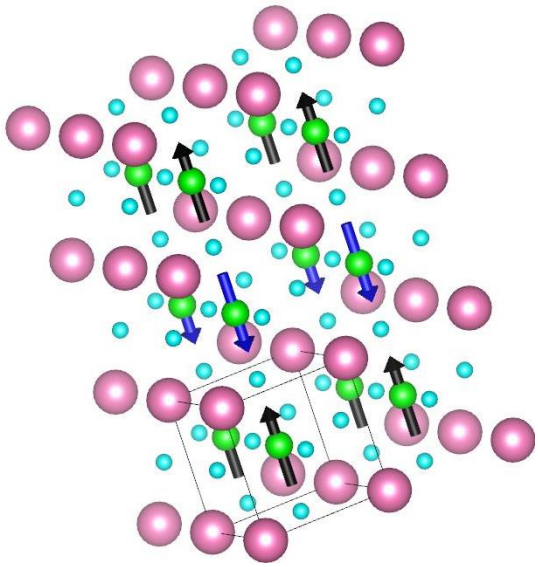

Fig.1.8 Ideal LMO is a type-A antiferromagnet

1.2.3 Double-exchange interaction

In 1951, Zener proposed a double exchange model [25], that is, the exchange interaction between the incompletely filled d-levels takes place by conducting electrons. This model can qualitatively explain the magnetism of some transitional metals and their alloys. Double-exchange is an exchange interaction between two transition metal ions with different valences, in which the oxygen atom acts as the intermediary.

Taking LSMO as an example, Mn in this material has two valences. Unlike the

superexchange, a p-electron of the oxygen atom enters Mn^{4+} and this Mn^{4+} ion becomes Mn^{3+}. On the other side an e_g electron is exchanged into the p-orbital of the oxygen atom, so this Mn^{3+} ion on contrary becomes Mn^{4+}. Since the electron in the ion is not yet half-filled, the transferred spin will be parallel to its own, vice versa for Mn^{3+} [24]. To conclude, exchange interaction will occur between two transition metal ions with different valences, thus ferromagnetism emerges.

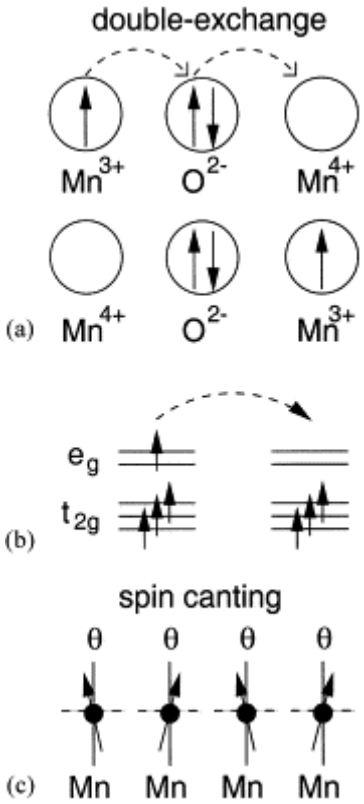

Fig.1.9 The change of valence in double exchange interaction, for Mn^{3+} and Mn^{4+}

1.3 Spin/charge/orbital ordered state in perovskite manganite

In the mixed valence compound system, the metal ions with different valences are arranged orderly in the lattice, which we call charge order, or Wigner lattice. Among the mixed valence manganates, the double-exchange between Mn^{3+} and Mn^{4+} is the most essential. Strong electron-JT phonon coupling and off-site Coulomb repulsion between valence electrons can lead to charge ordering [26]. When the ratio of Mn^{4+} is high or the radius of A-site ion is small, the charge order tend to appear, near the A-

doping with rational number of parameter x = 1/8，1/2，2/3，5/8，3/4，7/8, because the charge order is related to the heterostructure of the crystal. When x deviates from these rational numbers, a mixture of two adjacent phases is formed [27].

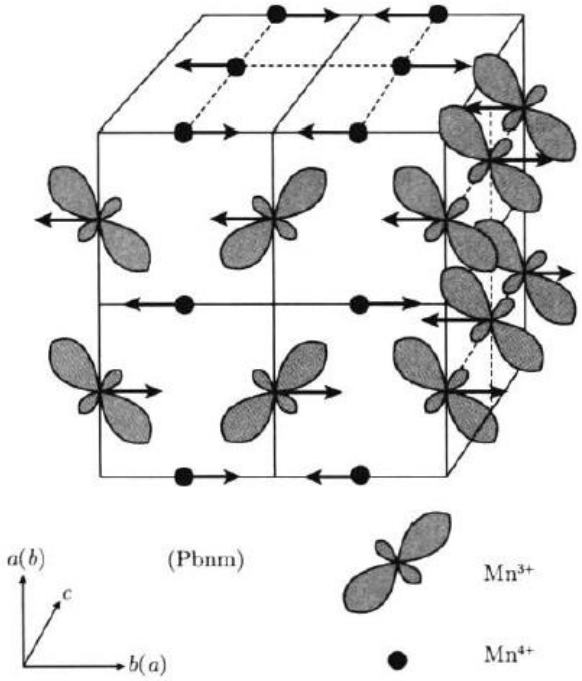

Fig.1.10 The charge/spin/orbit ordered structure of CE type antiferromagnets

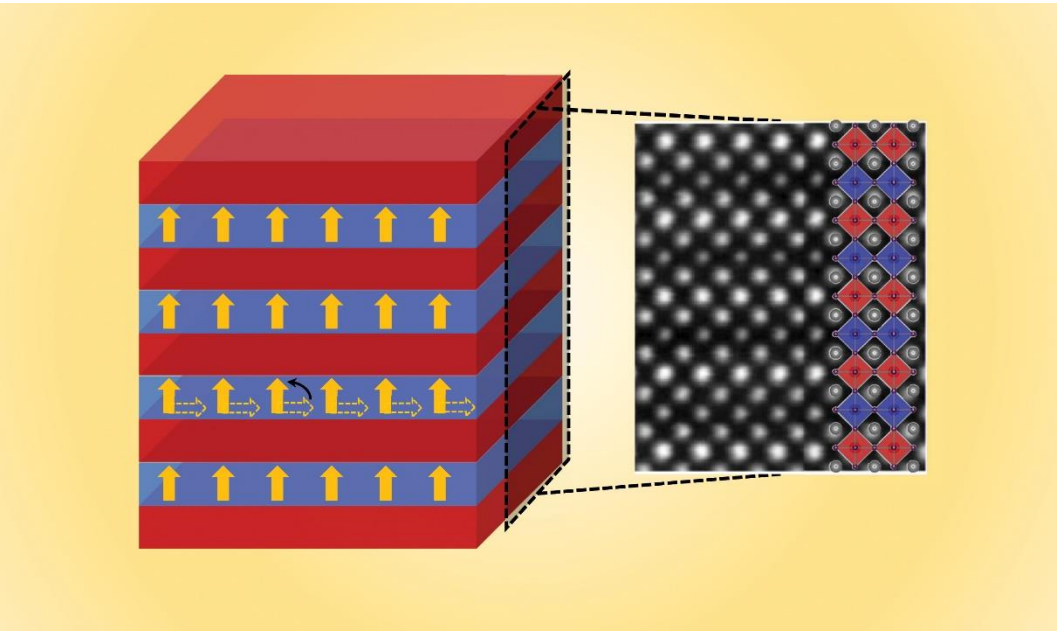

Fig.1.11 Spin arrangement of $(MnO_2)_2$ layers in LSMO, under Tc in magnetic field

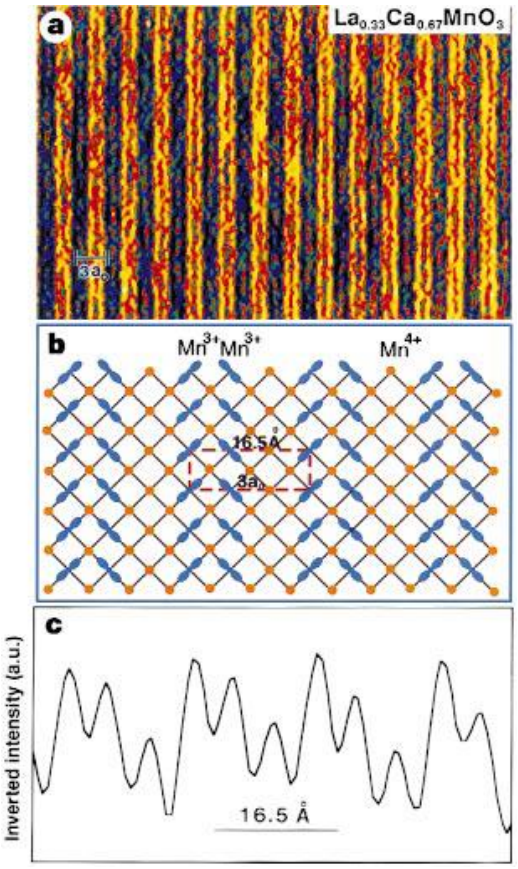

Fig.1.12 Charge ordering in LCMO

1.4 Exchange bias effect [28][29]

The exchange bias effect was first found by Meiklejohn and bean, in the Co nanoparticles coated by the CoO shells. In general, the hysteresis loop of ferromagnetic Co is symmetrical about the origin, but when the antiferromagnetic layer CoO is introduced and the temperature is lower than its Neel temperature, the hysteresis loop will shift along the opposite direction of the magnetic field, and at the same time with the increase of the coercive force, which is the so-called exchange bias effect, or say that the system is unidirectional anisotropic. The offset is called the exchange bias field, labelled as H_E [29]. The hysteresis loop is shown in Fig. 1.13. Generally speaking, the exchange bias effect comes from the unidirectional pinning effect of the antiferromagnetic layer on the ferromagnetic layer, i.e. it depends on the exchange coupling of the interfaces of ferromagnetic and antiferromagnetic layers.

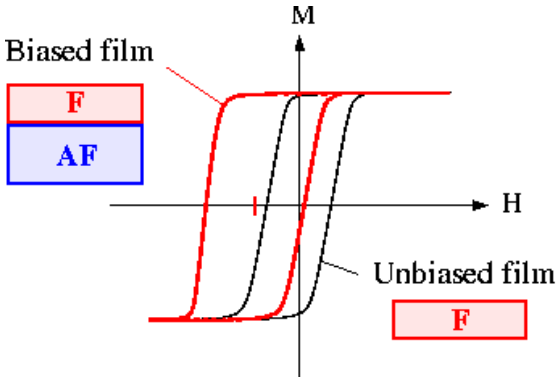

Fig.1.13 Exchange bias effect

Exchange bias is the macro manifestation of micro exchange interaction. In order to generate exchange bias, the system must contain at least two exchange coupling phases: one is reversible phase, i.e. its spin can be reversed in the external field; the other is fixed phase, which means its spin cannot be reversed in the range of external field in measurement. The exchange bias effect exists universally in the FM/AFM bilayer or interface. This structure contains many profound physical phenomena and characteristics, with complex physical connotation, which is the most widely studied exchange bias system at present, receiving great attention in both theory and application. Due to its great application prospects in many related fields, exchange bias effect is a hotspot of current research.

1.4.1 Physical image of exchange bias effect

In 1956, Meiklejohn and Bean proposed Meiklejohn-Bean model (M-B model) after discovering the exchange bias effect. It is believed in this model that the exchange bias effect can be qualitatively understood from the exchange coupling between interfaces in ferromagnetic/antiferromagnetic (FM/AFM) heterostructure [30]. The physical image is shown in Fig. 1.14.

According to M-B model, when $T_N<T<T_C$ (T_C: Curie temperature; T_N: Neel temperature), when an external magnetic field (larger than the saturation magnetic field of FM layer) is applied to this bilayer, the magnetic moment of the FM layer is oriented to the direction of the external field, showing an ordered state, while the AFM layer is still disordered. When $T<T_N$, in external field, due to the exchange coupling between

the interface of FM/AFM bilayer, the magnetic moment of the AFM layer at the interface will become parallel to that of the FM's, while when away from the interface, as in normal antiferromagnets, the magnetic moments are antiparallel between nearest neighbors. When the external field reverses, the magnetic moment of the FM layer follows with the field, while, however, since the exchange interaction in the AFM layer is pretty strong, its magnetic moment stays unchanged. However, due to the exchange interaction at the interface, FM's magnetic moment also tend to follow AFM's at the interface, so the exchange coupling at the interfaces should be overcome to reverse FM layer's magnetic moment, i.e. a large opposite magnetic field should be applied. When the magnetic field changes from the opposite direction to positive, because the magnetic moment of both layers are then parallel to the magnetic field. In this circumstance, even with a weak field, the magnetic moment of the FM layer could reverse. This phenomenon can be seen macroscopically as the shift of the hysteresis loop to the opposite direction of the external field, i.e. the exchange bias effect.

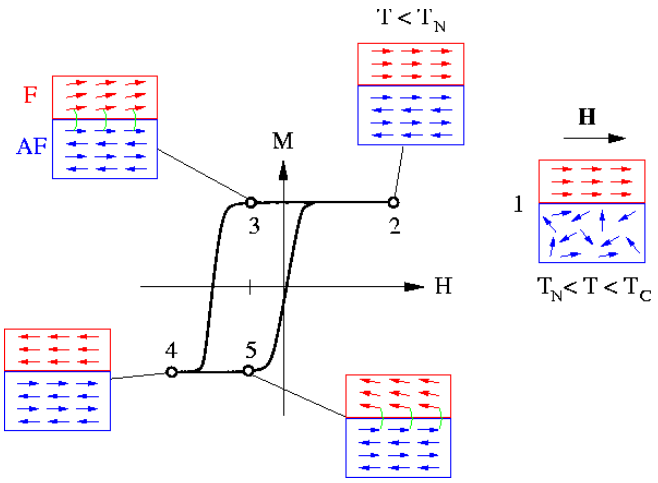

Fig.1.14 Exchange Bias effect in FM/AFM bilayer system

Meiklejohn and Bean also proposed a theoretical model for the exchange bias effect. They abstract the ferromagnetic layer and the antiferromagnetic layer as a single magnetization vector respectively, and can only rotate uniformly in the plane. The angular relationship of the magnetization vector is shown in Fig. 1.15, where H is the external magnetic field, α is the angle between the AFM's moment and y axis, β is the

angle between the FM's moment and y axis, and θ is the angle between the external magnetic field and y axis. Then the energy of the system can be expressed as

$$E = -HM_{FM}t_{FM}\cos(\theta-\beta) - HM_{AFM}t_{AFM}\cos(\theta-\alpha) + K_{FM}t_{FM}\sin^2(\beta) + K_{AFM}t_{AFM}\sin^2(\alpha) + J_{ex}\cos(\theta-\alpha) \quad (5)$$

Here M_{FM}/M_{AFM}, t_{FM}/t_{AFM}, and K_{FM}/K_{AFM} are the magnetization, thickness, and anisotropy constants of FM and AFM layers. J_{ex} is the energy of exchange interaction. The first two terms are the magneto-static energy between the external field and them; the third and fourth terms are their anisotropic energy; the last term represents the exchange interaction energy at interface.

To simplify the formula above, since the magneto-static energy between AFM layer and field is far less than its anisotropic energy, we have approximately $\alpha = 0$. If the anisotropy of the FM layer is ignored, and assume the direction of the magnetic field is the same as the anisotropic axis, then according to the least energy principle, we can get

$$H_E = \frac{J_{ex}}{K_{FM}t_{FM}} \quad (6)$$

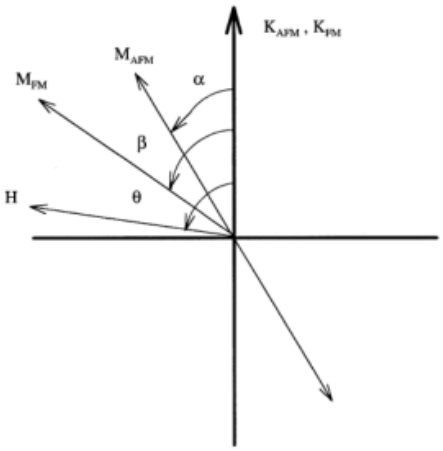

Fig.1.15 Relative angle of magnetic moments and field in exchange bias system

Formula (6) is an important conclusion of M-B model, which is in accordance with the previous empirical results, and the relationship between the exchange bias and the thickness of the antiferromagnetic layer could also obtained from it.

Although M-B model can qualitatively present the physical images of exchange bias, there are still many shortcomings. First of all, to take an effect on unidirectional pinning on FM layer. The model requires thick AFM layer and great anisotropy. In addition, the magnitude of exchange bias obtained by the M-B model is quite different from the experimental value, and cannot explain the experimental fact that exchange bias effect exists at the compensated AFM interface. With continuous research and development of exchange bias effect, a large number of models have been proposed. For example, Malozemoff's random field model solves the problem of great difference between M-B model and experimental value. Mauri's antiferromagnetic domain model solves the hypothesis of infinite anisotropy of antiferromagnetic layer in M-B model. Spin-flop model puts forward the theory of exchange bias caused due to random field generated by defects at interface, and the conclusion is better consistent with the experimental result than M-B model. Apart from these, there are many other models of exchange bias, each has its own limitations, and there are also contradictions between them. So, at present, some experimental phenomena about exchange bias effect have not been well explained, and there is not a perfect universal model to explain exchange bias effect.

1.4.2 Factors of exchange bias effect [29]

There are various factors that are responsible for exchange bias effect. On the one hand, it depends on the intrinsic properties of the system, such as the thickness of FM and AFM layers, size of grains, the anisotropy of the magneto-crystalline and the competition of the interface exchange coupling. On the other hand, it depends on external factors, such as temperature, the number of measurements and the intensity of cooling field. These many factors make the study of exchange bias effect very complex.

1.4.2.1 Thickness of ferromagnetic layer

It is found in research that for FM/AFM bilayer system, when the thickness of the AFM layer is constant and the thickness of FM layer is smaller than its domain wall,

the relationship between the exchange bias field and the thickness of FM layer is in accordance with the formula $H_E \propto \frac{1}{t_{FM}}$, i.e. in inverse proportion. This result proves that the exchange bias effect originates from the exchange coupling at the interface of FM/AFM bilayer, i.e. the M-B model. However, in the experiment, it is noticed that there are always some deviations in this relationship. There are approximately three reasons, one is that the thickness of FM layer cannot be accurately measured; the other is that the thin film synthesis technology cannot guarantee the continuity and uniformity; the third is that the domain walls parallel to the interface may be formed in FM layer.

In general, the coercive force decreases with the increase of FM layer's thickness, but the mechanism of coercive force is very complex, which is closely related to the growth quality, microstructure and defect distribution of FM and AFM layers, thus making the research on coercive force in FM/AFM bilayer system relatively complex.

1.4.2.2 Thickness of antiferromagnetic layer

Compared with FM layer, the relationship between the exchange bias field and the thickness of the AFM layer is much more complex. Generally, when the thickness is large, the exchange bias field remains unchanged; as it decreases, the exchange bias field will drop rapidly at a certain point. Finally, when the thickness reaches a certain critical value, the exchange bias field tends to zero. This is because when the thickness of AFM layer reaches this critical value, the anisotropic energy of it is smaller than the exchange interaction energy at the interface So in this case, the magnetic moment of AFM layer will also reverse during the reverse process of FM layer, i.e. AFM layer loses its pinning effect on FM layer. The macroscopic interpretation is that the exchange bias effect disappears in the hysteresis loop. The exchange bias field measured in FeMn/NiFe bilayer in accordance with AFM thickness is consistent with this explanation. Moreover, for different exchange bias systems, the critical AFM thickness is also variant due to the different anisotropy constants. Presently, since the net magnetic moment of antiferromagnetic material is very small, and the

antiferromagnetic structure itself is complex, the relationship between exchange bias and the thickness of AFM layer remains to be further studied.

1.4.2.3 Temperature

In most cases, with the increase of temperature, the influence of thermal disturbance on the exchange coupling goes up gradually. Therefore, with the increase of temperature, the exchange bias field decreases until at a certain temperature, exchange bias disappears completely. This temperature is called blocking temperature T_B. Generally speaking, T_B of antiferromagnetic materials is smaller than T_N, but for some materials they are close to each other. Additionally, it is reported that $T_B > T_N$ is observed in Co/CoO films.

1.4.2.4 Ferromagnetic/antiferromagnetic interface

The exchange bias effect strongly depends on the interface, so H_E is in strong accordance with the exchange coupling interaction at the interface of FM/AFM system. There are two permutations of the AFM moment at interface: the compensated moment and the uncompensated moment.

The M-B model points out that the exchange bias effect comes from the pinning effect of the AFM layer on the FM layer. So, there is no net magnetic moment in the AFM interface with compensate magnetic moment, thus cannot generate pinning effect on the FM layer. While a net magnetic moment exists at the interface without compensate magnetic moment, able to generate pinning effect. Taking the CoO (100) surface as an example, it has been proved experimentally that the exchange bias effect can be guaranteed when the antiferromagnetic moment at interface is not compensated. However, it is also found that for some compensated interfaces, there are also some tiny exchange bias effect, for example, in FeF_2(110)/Fe system. This may be due to the interface defects and other factors, contributing to the net magnetic moment of the interface, that is, some magnetic moments in the whole interface are not compensated.

§2 Experimental Methods

2.1 Pulsed Laser Deposition (PLD) [31]

In the 1960s, the invention of laser opened a new field of interaction between laser and matter. It was found that when we irradiate laser on a solid material, electrons, ions and neutral atoms will escape from the surface and form a luminescent plasma area nearby. Then people came up with an idea that, if these particles could deposit on the substrate, a thin film could be obtained, which the concept of laser coating. In 1965, Smith *et al.* first tried to prepare optical thin films by laser, but after analysis, it was found that this method was similar to the electron beam evaporation coating, and did not show great advantages, so the technology of growing thin films by laser at that time did not attract much attention. It was not until 1987, when Bell Laboratories in the United States successfully grow high-quality YBCO superconducting thin films by using short wavelength pulsed excimer laser for the first time, did Pulsed laser deposition (PLD) technology become an important film synthesizing technology, which has been highly valued by many international researchers. It is found that PLD has some advantages and potential in the preparation of superconductors, ferroelectrics, diamond or diamond-like carbon and organic films, and it has become a new widely used film synthesizing technique.

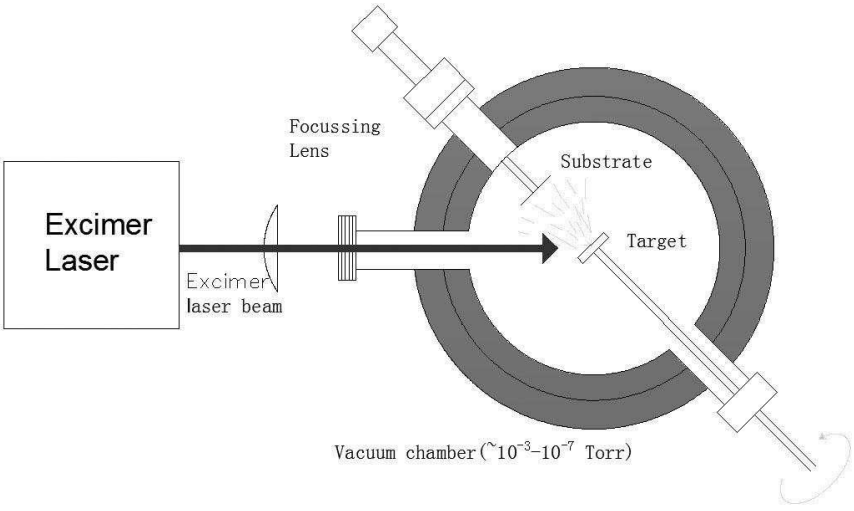

Fig.2.1 Pulsed laser deposition (PLD) system

The principle of PLD is to irradiate the high-power pulsed laser focused by lenses on the target surface, evaporate the target material by high temperature, and then generate high pressure plasma. The plasma dilates directionally in vacuum and deposits on the substrate to form a film [32]. Equipment for PLD technique is shown in Fig. 2.1.

The detailed process of PLD can be roughly divided into the following three steps:

First, high-power pulsed laser focuses on the target surface, producing extremely high temperature. When the temperature rises above target's vaporization temperature, the target evaporates. Due to the high laser energy, the vaporized atoms will ionize to produce plasma, macroscopically represented as bright plasmatic flame with an intense core. The interaction between the laser and the target plays a decisive role in the uniformity, crystal structure and composition of the film [33].

Then, the plasma flame with dense core formed on the target surface continues to ionize under the action of laser, with the temperature and pressure of plasma continuing to rise, a plasma plume is generated. The motion of plasma plume includes isothermal expansion and adiabatic expansion. The isothermal expansion occurs when the laser acts on the plume, and the adiabatic expansion occurs after that. In the process of plasma plume moving to the substrate, there will be a series of interactions with gas molecules, such as collision, scattering or vapor chemical reaction. The interaction in this process has an important impact on the quality and structure of the film [34].

Finally, the plasma plume reaches the substrate through, and these high-energy particles interact with the substrate to form a nucleus. With the continuous collision, the nuclei grow and finally contact with each other to form a film. Sometimes in order to improve the quality of the film, the substrate can be heated. In this process, the energy, velocity of the particles in the plasma plume, as well as the interaction between the particles and gas, have a considerable effect on the formation of the film.

There are many advantages of PLD technique:

First of all, when the high-power pulsed laser interacts with the target, all the atoms of the target evaporate together, with no preferential atoms, ensuring the consistency of the composition of the film and the target. The energy of laser pulse is high, enough to

evaporate infusible complex inorganic compounds, which solves the problem of growing refractory inorganic compound films.

Next, a variety of gases can be introduced to synthesis multi-component compound films.

Finally, the pulsed laser deposition technology has the advantages of fast reaction speed, fast film growth speed and short experiment period.

In addition, there are also many shortcomings in PLD technique, such as it is difficult to avoid the emergence of large particles or droplets in growth process, lowering the quality of the films, and the technology can only form a relatively uniform film in a small area, having difficulty in forming a uniform film in a large area.

There are many factors in PLD technology, including the following aspects:

1. Substrate temperature: Substrate temperature is essential for the quality of films. With high substrate temperature, the deposited atoms have high mobility, which helps crystallization.

2. Laser energy: Laser energy determines the particle size of film components. Each target corresponds to an energy threshold. Only when the energy of the pulsed laser is higher than the threshold can the target evaporate. Moreover, the difference in energy has a significant effect on the size of the target evaporation particles, so the choice of appropriate energy value is also a key to thin film growth.

3. Distance between the target and the substrate: In the process of plasma plume moving to the substrate, it will interact with gas molecules by such as collision, scattering and vapor chemical reaction. Therefore, the distance between the target and the substrate can adjust the energy and speed of particles in the plasma plume, and selecting the appropriate distance has an important influence on the crystallization and uniformity of the film.

4. Pressure of protective atmosphere: In general, gases of a certain pressure will be introduced into the vacuum chamber during the growth. One reason is that the gas may be required to participate in the reaction in growth. The other is that the protective atmosphere can play a role in regulating the plume.

5. Target density: if the target density is too small, the particles evaporated by pulsed laser may be large, which has a negative effect on the film quality.

To conclude, PLD is a technique considering a variety of factors, to adjust the parameters corresponding to these factors, find the best parameters and the best matching of these parameters, and use the best conditions to get films with good quality.

The PLD system used in this experiment is Neocera's Pioneer-120 PLD system. The laser is produced by 248nm KrF nanosecond laser generator.

2.2 Physical Property Measurement Method

2.2.1 X-ray Diffraction (XRD)

X-ray diffraction (XRD) is a commonly used method to characterize the structure of materials. It has a wide range of research objects, including bulk materials, powders and thin films. X-ray diffraction has the advantages of non-destructive measurement, no pollution and fast measurement speed. The crystal structure, orientation and cell parameters of the sample can be obtained by XRD. Especially for thin films, the interface roughness and thickness of the films can also be precisely obtained. X-ray diffraction has an inevitable advantage in the study of physical properties of 1-100nm ultra-thin films.

The principle of XRD follows Bragg formula, i.e. $2d\sin\theta = n\lambda$, where n is the diffraction series, λ is the wavelength of X-ray, d is the crystal plane spacing, and θ is the incident angle. When X-ray hits the surface with incidence angle θ, due to the periodicity of the atoms in the crystal, and the scattering waves of each atom interfere with each other, and the diffraction waves are formed by coherent enhancement in some fixed directions. The results of XRD correspond to the crystal structure one by one in reciprocal space. The diffraction intensity is mainly related to the type and position of atoms in the cell, while the diffraction direction is mainly determined by the shape and size of the crystal cell.

2.2.2 X-ray reflection (XRR)

XRR, also known as X-ray reflectometer, is a non-contact, non-destructive analysis technology to determine the thickness, density, roughness and gap roughness of the film. When the X-ray irradiates the sample at a very small angle, it is completely reflected. As the irradiation angle increases, when it exceeds a critical angle, which depends on the material. X-rays reflect from the sample's interface and generate interference fringes. The periodicity of the fringes is directly proportional to the thickness of the film, the decrease of the intensity is directly proportional to the roughness of the film, and the amplitude of the fringes is directly proportional to the density of the top and bottom layers. The typical equipment of XRR experiment is shown in Figure.2.2. The monochromator, analyzer crystal, Soller slit and knife edge collimator are used to adjust the configuration to optimize the measurement conditions matching the sample.

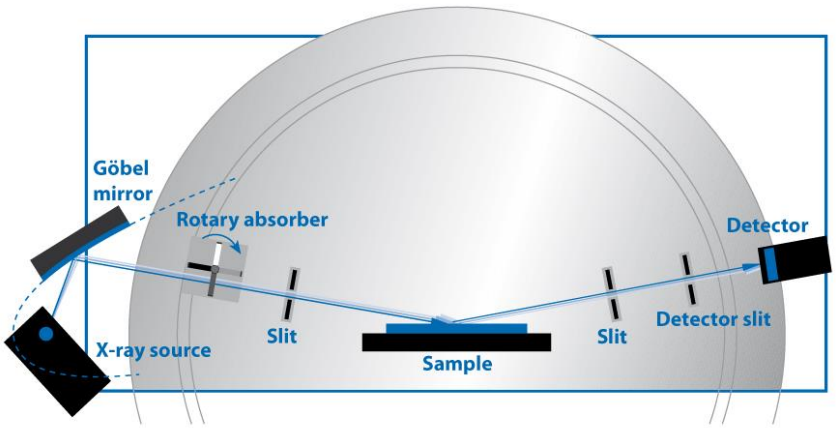

Fig.2.2 XRR measurement system

2.2.3 Comprehensive physical property measurement system (PPMS)

PPMS is an instrument developed by Quantum Design company of the United States, to conduct research on various physical properties of materials. The concept of PPMS system is to integrate all kinds of automatic physical property measurement methods, such as magnetism, electricity, thermology and morphology, and evenferroelectricity and dielectricity, on a perfectly controlled platform of extremely low temperature (50mK) and strong magnetic field (±16T), in order that the low

temperature and strong magnetic field environment of the system can be fully utilized.

Fig.2.3 Physical Property Measurement System (PPMS)

A PPMS system consists of a fundamental system and various measurement and expansion function options: The fundamental system provides a low temperature and strong magnetic field environment, as well as the software and hardware control center of the whole system. For most conventional experiment projects, PPMS has designed fully automatic measurement software and hardware with standard measurement functions, such as resistivity, magnetoresistance, differential resistance, Hall coefficient, V-I characteristics, critical current, AC susceptibility, hysteresis loop, specific heat, thermomagnetic curve, thermoelectric effect, Seebeck coefficient, thermal conductivity and morphology characterization, etc. The reliability and convenience of these measurement methods have been approved by the world scientific community in the past decade. By unique and ingenious design, all kinds of measurement options on PPMS system work without interference, and can quickly switch to each other.

In addition, the PPMS system has reserved a perfect software and hardware interface, so that users can control the third-party equipment through the PPMS system, and use the low-temperature and strong magnetic field environment and measurement functions of the PPMS system to carry out experiments designed by users themselves, such as the measurement of ferroelectricity, dielectricity, electric transport with optical

or microwave radiation, magnetic measurement under electric field induction and magnetoelectric coupling.

2.2.4 X-ray photoelectron spectroscopy (XPS)

XPS uses X-ray to irradiate the sample, to excite the inner electrons or valence electrons. The electrons excited by photons are called photoelectrons. The photoelectron spectroscopy can be made by measuring the energy of photoelectrons, with the kinetic energy of photoelectrons as the abscissa and the relative intensity (pulses per second) as the ordinate, to obtain information about the composition of the measured object. XPS is mainly used to realize the qualitative analysis of surface elements, including valence states by determining the binding energy of electrons. Since XPS is most useful for chemical analysis, it is also called electron spectroscopy for chemical analysis

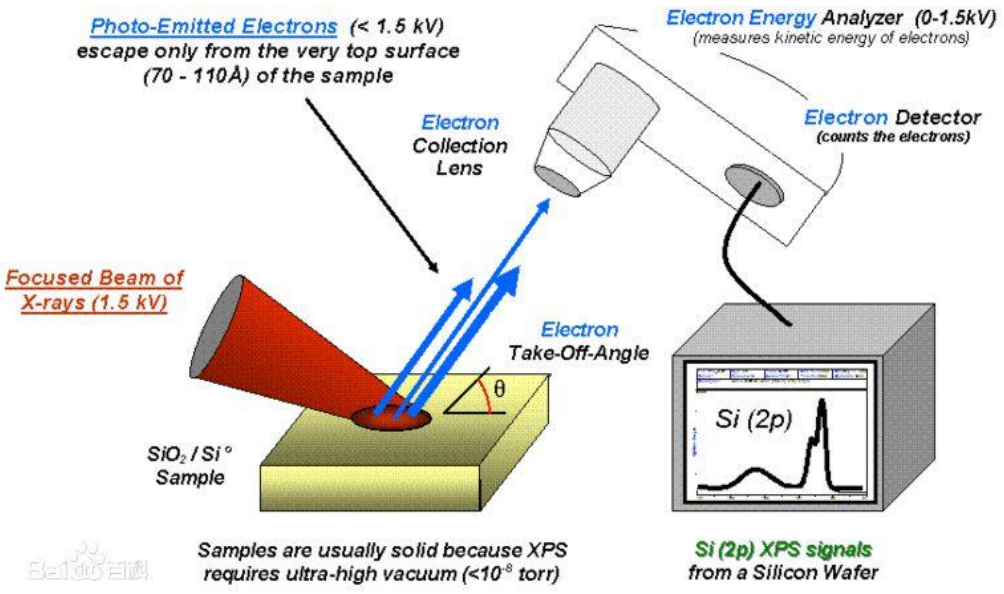

Fig.2.4 X-ray photoelectron spectroscopy (XPS) equipment

General measurement purposes are as follows:

1. Qualitative analysis of elements. All elements except H and He can be identified according to the position of the characteristic lines in the spectrum.

2. Quantitative analysis of elements. According to the intensity of photoelectrons (the area of the photoelectron peak) in the spectrum, the atomic content or relative concentration can be reflected.

3. Surface analysis of solid. It includes the chemical or element composition of the surface, valences of atoms, surface state, distribution of the electron cloud, and the energy levels of the surface electrons.

4. The structure of the compound. It can accurately measure the chemical shift of the binding energy of the inner electrons, and provide the information of bond and charge distribution.

The method can be used to measure the elements and their contents with 1-12nm of the sample's surface, detect the surface impurities, the experimental chemical formula of material containing excessive surface impurities, the state of one or more elements in the sample, the bond energy of one or multiple states, the thickness of single or multi layers within 12nm at the surface of different materials, and the density of states, etc.

2.2.5 Electron beam Irradiation

The basic principle of electron beam processing is: the electrons emitted from the hot filament cathode in vacuum are accelerated to a high speed under the action of a high voltage, and then converge into a high-power density electron beam through the electromagnetic lens. When impinging on the workpiece, the kinetic energy of the electron beam immediately changes into heat, producing extremely high temperature, which can be used for welding, piercing, grooving and cutting. Due to the energy loss and scattering when the electron beam collides with the gas molecules, the processing is usually carried out in vacuum. The electron beam processing machine is composed of electron gun which produces electron beam, bunching coil which controls electron beam, deflection coil which controls the electron beam to scan, power supply system, vacuum chamber where workpiece is placed, and observation device.

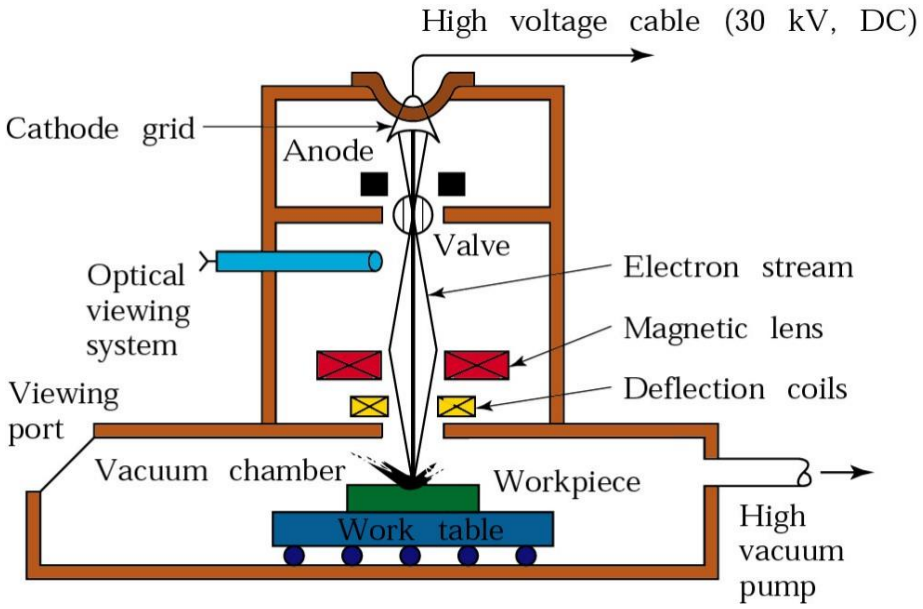

Fig.2.5 Electron beam processing

The major characteristics of electron beam irradiation are the high special concentration, high power density of the electron beam, no mechanical contact, no tool loss, and fast processing speed.

The main disadvantages are: due to the use of high voltage, intense X-rays are generated, so corresponding safety measures must be taken; the need of vacuum device for processing and the high cost of equipment.

§3 LMO thin film preparation, electron beam heating, and its effect on magnetic properties

3.1 Selection of LMO thin film growth condition

In this experiment, high quality LMO thin films were grown using PLD on $SrTiO_3$ (001) substrate with TiO_2 termination. STO single crystal substrate is cubic symmetric, with lattice constant a=3.91Å. LMO has tetragonal symmetry, with lattice constant a=b=3.98Å, c=3.85Å, and the mismatch with substrate is 1.5%. The unrelaxed epitaxial film should be under tensile strain, and the stress will reduce the c-axis lattice constant of LMO and cause distortion, which will affect the crystal structure and corresponding magnetic properties of LMO. Therefore, before the electron beam processing of LMO films, we should select the appropriate preparation conditions in advance, to obtain the LMO films with the required structure.

Through a lot of experiment optimization to the growth conditions of LMO thin films, in the following experiment, the best preparation parameters were selected, that is: substrate temperature 740℃, oxygen pressure 30 Pa, laser energy 120 mJ per pulse, and pulse frequency 1 Hz. In order to determine the optimal thickness of LMO films, the deposition time of 30, 20, 10, 5, and 2 minutes were tested. Then, the crystal structure of the films was characterized by XRR and XRD, and the magnetic properties were measured by PPMS.

Take the film with a deposition time of 30 minutes as an example, as shown in Fig. 3.1 is the XRR test result. The result of XRR fit shows that the thickness of LMO film is about 20 nm. Analogously, ignoring the change of lattice constant, the thickness of the five samples should be about 20, 13, 7, 3, and 1nm.

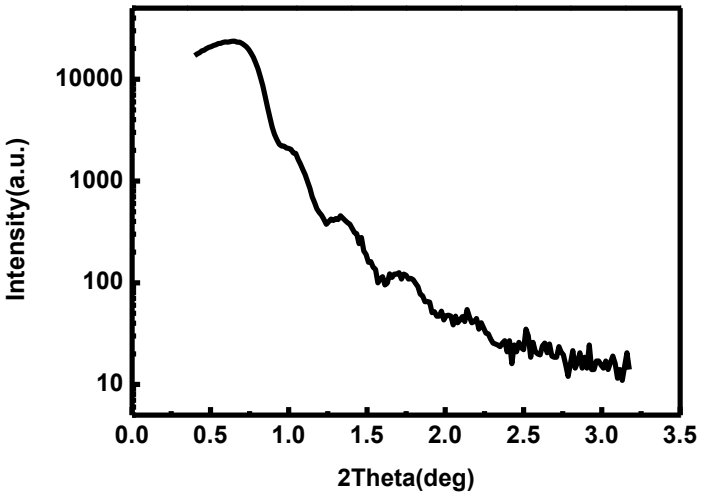

Fig.3.1 XRR data for LMO films with deposition time of 30 minutes

As shown in Fig. 3.2, the XRD spectrums of LMO are measured near the main peak of STO (001), with a scanning range of 20° to 25°. The characteristics of XRD and XRR show that LMO has good epitaxial growth and sharp interface along STO (001) direction.

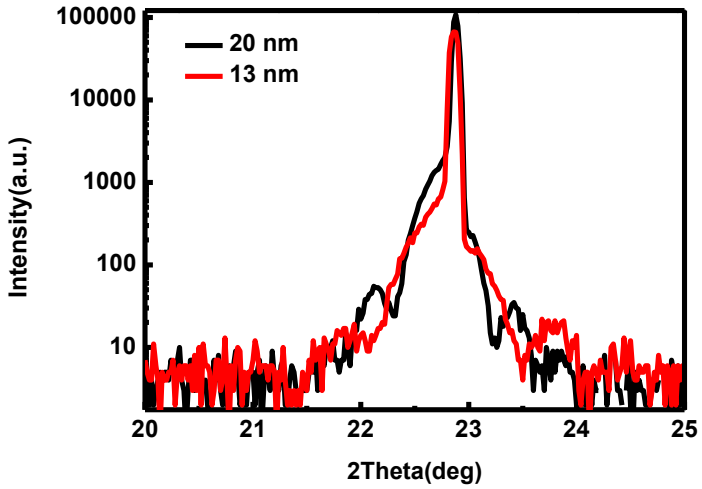

Fig.3.2 XRD spectrum of LMO films

Fig. 3.3 shows the relationship between the magnetic moment per unit cell and the temperature of LMO film with different thickness, measured by PPMS. It can be inferred that the polarizability of film thickness 20nm and 13nm are basically 100% at

low temperature, and the Curie temperatures of 20, 13 and 7nm films are generally the same, so it can be implied that the stress has been relaxed at 13nm, and the surface is normal LMO lattice.

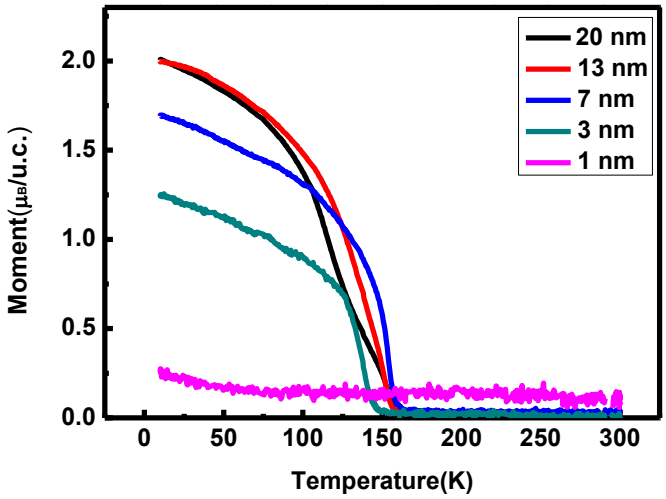

Fig.3.3 The relationship between the magnetic moment per unit cell, and the temperature of LMO film with different thickness

To sum up, the LMO films with deposition time of 20 minutes under the above conditions were selected as samples for electron beam irradiation and subsequent magnetic properties comparison.

3.2 Electron beam heating and its effect on magnetic properties

3.2.1 Conditions for electron beam irradiation

The parameters of electron beam irradiation chosen in this experiment: filament current 18.5A, bias voltage 10V, high voltage 1000V, electron beam current 0.5mA, beam sealing current 10mA, focusing current 304mA, and irradiation time 10min.

3.2.2 Changes on magnetic properties of LMO thin films after electron beam irradiation

Fig. 3.4 and Fig. 3.5 show the M-T images and hysteresis loops at different temperatures of LMO films before and after e-beam irradiation measured by PPMS.

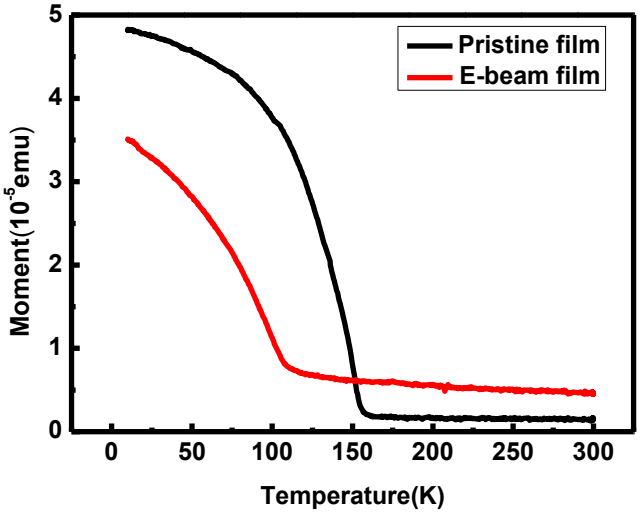

Fig.3.4 M-T plots of LMO thin films before and after electron beam irradiation

It can be seen from Fig. 3.4, that the Curie temperature before irradiation is about 155K, and there is no ferromagnetism after the phase transition point, which conforms to the ferromagnetic property of the oxygen-rich $LaMnO_{3+\delta}$ material. After irradiation, there are several variants: Curie temperature goes down to about 105K, the magnetism decreases at low temperature compared with before, and the films stays magnetic at high temperature.

From Fig. 3.5 we can see that the LMO film has only ferromagnetic phase before electron beam irradiation, but has mixed phases after irradiation. And the coercive force increases significantly. Meanwhile, the negative exchange bias effect was also observed at 10K.

Presented in Figure 3.6 is the changes of coercive force with respect to temperature before and after irradiation. Before processing, there was only ferromagnetic phase in LMO, and the coercive force increased with the decrease of temperature below Curie temperature. After irradiation, ferromagnetic phases exist before and after the phase transition point of LMO's ferromagnetic phase, and a minimum of coercive force appears near the phase transition point.

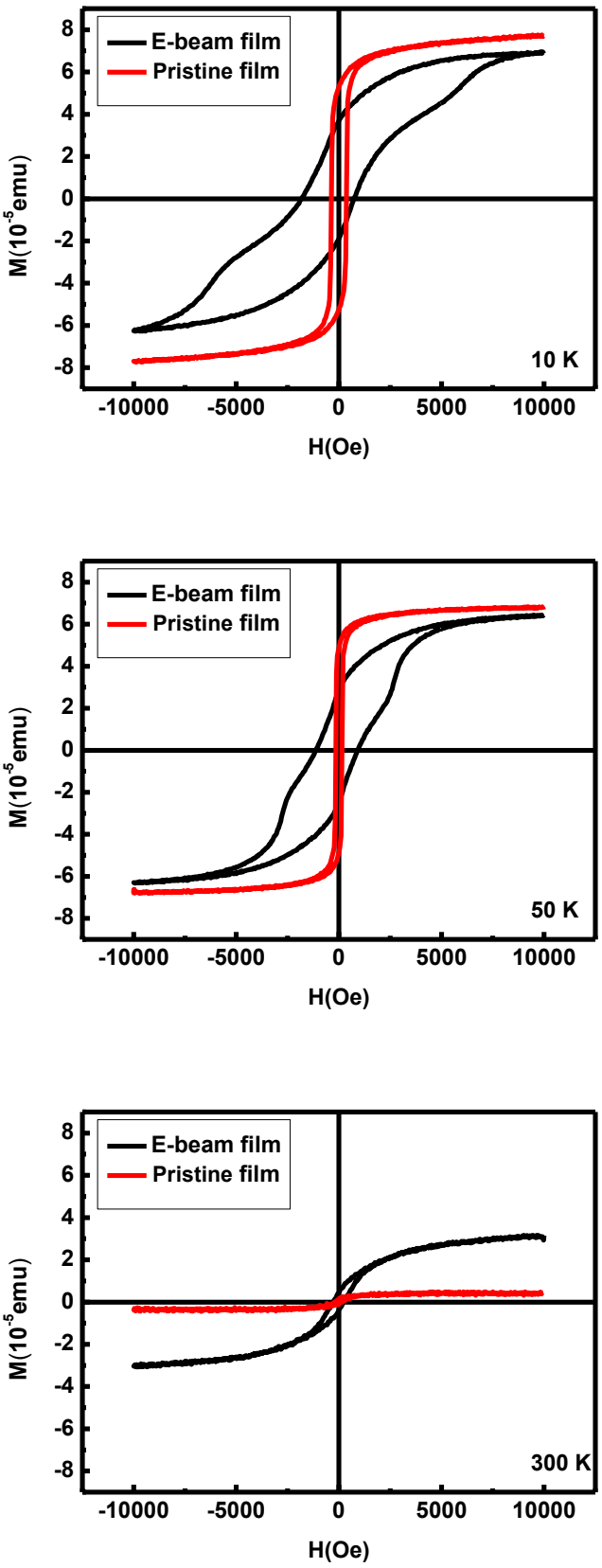

Fig.3.5 Hysteresis loops of LMO film before and after electron beam irradiation

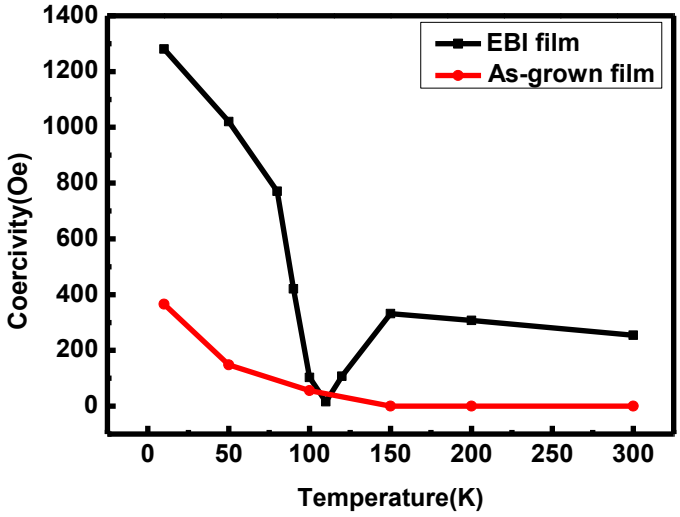

Fig.3.6 The relationship between coercive force and temperature of LMO film before and after electron beam irradiation

3.2.3 XPS measurement of LMO thin films before and after electron beam irradiation

Because the magnetic properties of LMO class materials are related to the valence of Mn, in order to explain the changes in magnetism of LMO films after electron beam irradiation, the XPS analysis of the two samples was carried out. Fig.3.7 shows the XPS spectra and fitting results of Mn2p and O1s electrons of LMO film before and after electron beam irradiation. It is apparent that the ratio of Mn^{3+} and oxygen vacancies increased significantly after irradiation.

Samples	Mn^{4+} / Mn^{3+}	Lattice Oxygen / Oxygen vacancies
As-grown films	1.145	1.118
EBI films	0.746	0.804

Table 3.1 The ratio of ions, before and after irradiation, from XPS data

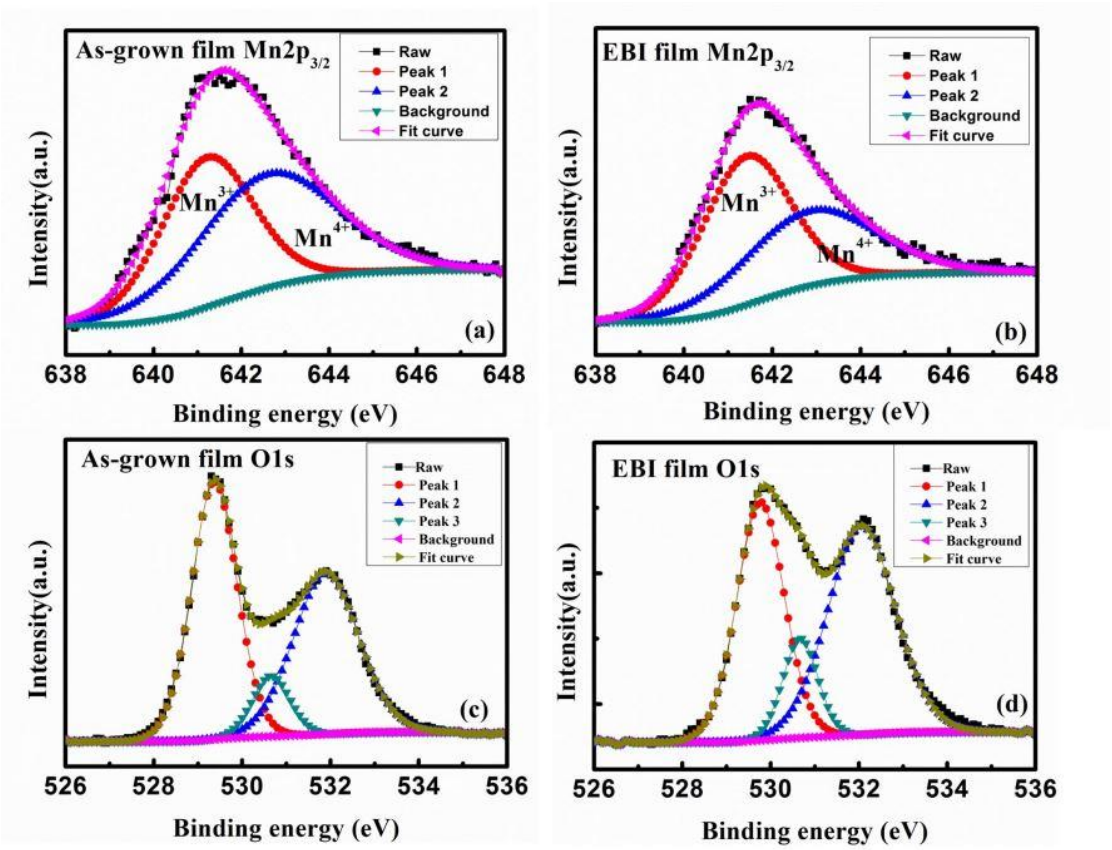

Fig.3.7 XPS data of Mn2p and O1s of LMO films, before and after irradiation

3.2.4 STEM line scan of Sr

At present, only STEM line scans of Sr element of the irradiated sample, in directions perpendicular to and across the film, as well as parallel to and inside the film, are carried out. The results indicate that Sr diffuses obviously into the LMO film, and the diffusion intensities at the same depth throughout the film are basically the same. Therefore, LSMO transition layer is formed at the LMO/STO interface after irradiation, and even the whole film may become heterogeneous doped LSMO. Therefore, LSMO ferromagnetic phase may also exist at this time. Since the original sample hasn't been measured in the same way, and the measurement of Ti element has not been carried out yet, the specific composition of the film after irradiation and whether it is electron beam irradiation that causes the diffusion of Sr still requires further experimental verification. However, from the initial XRD and XRR results, the interface of the film should be very sharp, and it is speculated that there is no diffusion in the initial state.

3.3 Analysis and discussion of experimental data

It can be seen from the XPS results that there are both Mn^{3+} and Mn^{4+} ions before the electron beam irradiation. Therefore, the LMO film used in this experiment is an oxygen-rich $LaMnO_{3+\delta}$ film. If other possible factors are not considered, $\delta \approx 0.255$. After irradiation, the ratio of Mn^{4+} is less than a half, $\delta \approx 0.214$.

For the phenomenon of magnetism weakening of the film at low temperature, after irradiation, it can be explained that the increase of the ratio of Mn^{3+} ions lead to the decrease of ferromagnetic composition caused by the double-exchange interaction of Mn^{3+}-Mn^{4+} in the film, while the antiferromagnetic composition by the superexchange of Mn^{3+}-Mn^{3+} increase. In total, the magnetism is weakened.

At high temperature or even room temperature, the ferromagnetism of the irradiated sample still exists. Presently it is speculated that diffusion occurs at the LMO/STO interface, forming a transition layer of LSMO or other components. At high temperature, although the ferromagnetic phase of LMO itself disappears, due to the high Curie temperature of the transition layer about interface, there is still ferromagnetic phase, so a certain intensity of magnetism remains.

This conjecture can also be proved on the hysteresis loop. In hysteresis loops at 10K and 15K, it can be inferred that the film before irradiation has no exchange bias, and has only a ferromagnetic phase, and there should be no diffusion at the interface. However, at 10K, the negative exchange bias is obvious for irradiated sample and the hysteresis loop has a clear turning point. Therefore, there should be two ferromagnetic phases in the irradiated sample at 10K and 50K, one is LMO itself, the other may be caused by the diffusion at the interface, and there is also LMO antiferromagnetic phase below one at a temperature $10\mathrm{K} < T_{\mathrm{N}} < 50\mathrm{K}$, which causes the exchange bias effect. At room temperature, it is obvious that there is residual ferromagnetism in the irradiated sample. Meanwhile, the increase of coercive force may be due to complexity of the structure and composition of the film after irradiation, which changes some properties of the magnetic domain, and the exchange bias effect. The true reasons require further study.

For the phenomenon that a minimum of the coercive force appears around the phase transition point, with a value almost 0, we should first notice that spin-glass state tend to appear near the phase transition, resulting in an extreme value, and since the interface between the two ferromagnetic phases in this experiment is vague, the ferromagnetic phase by diffusion is probably affected by the LMO's ferromagnetic phase. As a result, such phase almost does not emerge near the transition point, but reappears gradually after transition without the influence of LMO ferromagnetic phase. If LMO/LSMO is measured in the same way, to get a minimum value obviously non-zero, then this minimum value is related to the fuzzy interface. The specific reasons need to be further explored.

3.4 Conclusion

It can be concluded from the above discussion, that electron beam irradiation can easily and effectively adjust the stoichiometric number of O in LMO thin films, then modify the magnetic properties, the appearance of exchange bias effect, the value of coercive force, etc. However, at the same time, it may also lead to diffusion at the interface, which complicates the structure.

§4 Outlook

The magnetic properties of perovskite manganate can be controlled by doping and adjusting the stoichiometry of oxygen. Compared with doping, the method of changing the stoichiometric number of O in LMO by electron beam irradiation is clearly more convenient. This method starts with one kind of sample, and may be more suitable for large-scale production by adjusting the magnetic properties of the sample through irradiation time and other conditions. In the next step, we can study whether different irradiation time will lead to different properties for the same sample, and whether we can directly and precisely get the product with desired magnetic properties, by adjusting the irradiation conditions. In the same way, it is also worth trying whether the surface magnetism of the sample can be fine processed by ultra-thin electron beam irradiation. As for the interface diffusion problem, we need to find another way to make it more controllable.

Biblography

[1] Maeno Y, Hashimoto H, Yoshida K, et al. Superconductivity in a layered perovskite without copper [J]. Nature, 1994, 372(6506):532-534.

[2] Jin Z, Tang W, Zhang J, et al. Giant magnetoresistance in mechanical alloyed $La_{0.7}Sr_{0.06}Ca_{0.24}MnO_3$, perovskite [J]. Journal of Magnetism & Magnetic Materials, 1998, 187(2):237-241.

[3] Samoilov A V, Yeh N C, Vasquez R P. Anomalous Hall Effect in a Ferromagnetic Rare-Earth Cobalite [J]. 1996.

[4] Kundu A K, Ranjith R, Pralong V, et al. A Multiferroic Ceramic with Perovskite Structure [J]. Applied Physics Letters, 2008, 93(5):052906 - 052906-3.

[5] Jianwang C. Application principle of magnetoelectronic devices [J]. Physics Progress, 2006, 26(2):180-227.

[6] Tokura Y, Tomioka Y, Kuwahara H, et al. Magnetic-field-induced insulator-metal phenomena in perovskite manganese oxides [J]. Physica C Superconductivity, 1996, 263(1–4):544-549.

[7] Mizokawa T, Fujimori A. Spin, charge, and orbital ordering in Mn perovskite oxides studied by model Hartree-Fock calculations [J]. Physical Review B, 1997, 56(2):R493-R496.

[8] Renner C, Aeppli G, Ronnow H M. Charge ordering, stripes and phase separation in manganese perovskite oxides: An STM/STS study [J]. Materials Science & Engineering C, 2005, 25(5):775-778.

[9] Jahn H A, Teller E. Stability of Polyatomic Molecules in Degenerate Electronic States. I. Orbital Degeneracy [J]. Proceedings of the Royal Society of London, 1937, 161(905):220-235.

[10] Jonker G H, Santen J H V. Ferromagnetic compounds of manganese with perovskite structure [J]. Physica, 1950, 16(3):337-349.

[11] Goldschmidt V.M. The laws of crystal chemistry [J]. Naturwissenschaften, 1926, 14(21):477-485.

[12] Hwang H Y, Cheong S W, Radaelli P G, et al. Lattice Effects on the Magnetoresistance in Doped $LaMnO_3$ [J]. Physical Review Letters, 1995, 79(8):914-917.

[13] Daosheng D. The Fundamental Material Magnetism [M]. Beijing: Peking University Press, 2016:105-109.

[14] Heisenberg W. On the Theory of Ferromagnetism [J]. Zeitschrift fur Physik, 1928, 49:619-636.

[15] Faulkner J S. Constructing the Spin Hamiltonian for an N-Electron System [J]. Phys Rev, 1962, 128.

[16] Daosheng D, Kunming Q. Ferromagnetism (I) [M]. Beijing: Peking University Press, 1992:199-204.

[17] Daosheng D. The Fundamental Material Magnetism [M]. Beijing: Peking University Press, 2016:66-70.

[18] Slater J C. Atomic Shielding Constants [J]. Physical Review, 2008, 36(1):57-64.

[19] Weiss P R. The Application of the Bethe-Peierls Method to Ferromagnetism [J].

Physical Review, 1948, 74(10):1493-1504.

[20] Stuart R, Marshall W. Direct Exchange in Ferromagnets [J]. Physical Review Superseded in Part by Phys.rev.a Phys.rev.b Solid State Phys.rev.c & Phys.rev.d, 1960, 120(2):353-357.
Freeman A J, Watson R E. Theory of Direct Exchange in Ferromagnetism [J]. Physical Review, 1961, 124(5):1439-1454.

[21] Daosheng D, Kunming Q. Ferromagnetism (I) [M]. Beijing Peking University Press, 1992:208-235.

[22] Kramers H A. On the classical theory of the spinning electron [J]. Physica, 1934, 1(7):825-828.

[23] Anderson P W. Antiferromagnetism. Theory of Superexchange Interaction [J]. Physical Review, 1950, 79(2):350-356.

[24] Daosheng D. The Fundamental Material Magnetism [M]. Beijing: Peking University Press, 2016:88-92.

[25] Zener C. Interaction between the d-Shells in the Transition Metals. II. Ferromagnetic Compounds of Manganese with Perovskite Structure [J]. Physical Review, 1951, 82(3):403-405.

[26] Zhengkuan J, Guanghan C. Magnetoelectronics. Zhejiang University Press. 2005:230~233, 222~229.

[27] Mori S, Chen C H, Cheong S W. Pairing of charge-ordered stripes in (La,Ca)MnO_3[J]. Nature, 1998, 392(6675):473-476.

[28] Hongru Q. Spintronics. Beijing: Science Press. 2013:498-526.

[29] Shiming Z, Heyin L, Shujuan Y, et al. Exchange bias in FM/AFM bilayer [J]. Physics Progress, 2003, 23(1):62-81.

[30] Nogués J, Schuller I K. Exchange bias [J]. Journal of Magnetism & Magnetic Materials, 1999, 192(2):203-232.

[31] Gaomian G, Changyue C, Yongcang W, et al. Researches on Pulsed laser Deposition (PLD) Technology and Its Applications [J]. Journal of Air Force Engineering University Natural Science Edition, 2005, 6(3):77-81.

[32] Shin Y T, Shin S W, Shin J, et al. Pulsed laser deposition of a thin conjugated-polymer film [J]. Thin Solid Films, 2000, 360(1-2):13-16.

[33] Chrisey D B, Hubler G K. Pulsed Laser Deposition of Thin Films [M]. New York: Wiley, 1994

[34] Hastie J W, Bonnell D W, Paul A J, et al. Gasdynamicsand Chemistry in The Pulsed Laser Deposition of Oxide Dielectric Thin Films [J]. Mrs Online Proceeding Library, 1992, 302-334

Acknowledgement

This thesis is completed under the guidance of Professor Jinbo Yang. Mr. Yang is rigorous, enterprising, approachable, and accomplished in scientific research. He has given me great encouragement and support in both scientific research and life. From the topic selection, experimental design, data processing, theoretical analysis, to the thesis writing, all these are with the efforts of Prof. Yang. I would like to express my heartfelt thanks to him. In the future, I will benefit a lot from Mr. Yang's profound knowledge, rigorous attitude towards learning, and practical and hard-working professionalism.

Thanks for Mingzhu Xue's guidance in the whole process of graduation project. Every experiment detail and every data can't be separated from your patient instruction, and repeated explanation to the principle and phenomenon. Your enthusiasm for scientific research and cheerful personality are enjoyable in the process of experiment, so I soon got familiar with the laboratory.

In the end, I would like to say thanks my parents for their support and encouragement, for all they have done for me over these years, and for all the people who care about me.

Statement of Originality and Authorization for Use of Dissertation of Peking University

Statement of Originality

I solemnly declare that: The submitted dissertation is the result of my independent research under the guidance of my supervisor. Except for the quoted contents, this paper does not include any other works or achievements that have been published or written by individuals or groups. Individuals and groups who have made important contributions to the study of this paper have been clearly identified in this paper. The legal result of this statement shall be borne by myself.

Signature of the Author: Hao Li Date: May, 2018

Statement of Authorization for Use of Dissertation

I fully understand the regulations of Peking University on the collection, preservation and use of dissertations, namely:

- In accordance with the requirements of the university, submit the printed and electronic versions of the dissertation;
- The university has the right to keep the printed and electronic versions of the dissertations, provide directory retrieval and reading services, and provide services on the campus network;
- The school can use photocopying, reduction, digitization or other means to save papers;
- Due to some special reasons, it is necessary to delay the release of the electronic version of the dissertation, and the school is authorized to publish it in full on the campus network after □ one year / □ two years / □ three years.

(The confidential paper shall comply with this regulation after decryption)

Signature of the Author: Hao Li Signature of the Supervisor: Jinbo Yang

Date: May, 2018